

# Instrumental distortions in quantum optimal control

Uluk Rasulov<sup>1</sup> and Ilya Kuprov<sup>2,1,\*</sup>

*<sup>1</sup>School of Chemistry and Chemical Engineering,  
University of Southampton, United Kingdom.*

*<sup>2</sup>Department of Chemical and Biological Physics,  
Weizmann Institute of Science, Israel.*

## Abstract

Quantum optimal control methods, such as gradient ascent pulse engineering (GRAPE), are used for precise manipulation of quantum states. Many of those methods were pioneered in magnetic resonance spectroscopy where instrumental distortions are often negligible. However, that is not the case elsewhere: the usual jumble of cables, resonators, modulators, splitters, amplifiers, and filters can and do distort control signals. Those distortions may be non-linear, their inverse functions may be ill-defined and unstable; they may even vary from one day to the next, and across the sample.

Here we introduce the response-aware gradient ascent pulse engineering (RAW-GRAPE) framework, which accounts for any cascade of differentiable distortions within the GRAPE optimisation loop, does not require filter function inversion, and produces control sequences that are resilient to user-specified distortion cascades with user-specified parameter ensembles.

The framework is implemented into the optimal control module supplied with versions 2.10 and later of the open-source *Spinach* library; the user needs to provide function handles returning the actions by the distortions and, optionally, parameter ensembles for those actions.

*\*Email: ilya.kuprov@weizmann.ac.il*

## 1. Introduction

Gradient ascent pulse engineering (GRAPE) [1] and its extensions [2-5] are currently the dominant quantum optimal control frameworks in magnetic resonance spectroscopy [6,7] and imaging [8], and increasingly in other quantum process control applications [9], a notable recent example being atom interferometry [10,11]. All published GRAPE implementations assume that control sequence distortions by instrument filter functions are negligible. With one recent exception [5], all software implementations also use the piecewise-constant approximation for the control Hamiltonian without worrying about edge effects. In high-field liquid state nuclear magnetic resonance (NMR) those are indeed negligible [12], but elsewhere in quantum device engineering that is not the case [13].

The reason why minor distortions can be ignored is the definition of the GRAPE optimum: a zero gradient of the fidelity with respect to the control sequence [1] implies first order resilience to variations thereof. In benign cases (magnetic resonance [6,14], atom interferometry [10,11]), optimal control theory yields impressive results right out of the box. However, in low- $\gamma$  NMR and in time domain electron spin resonance (ESR) hardware distortions of the control sequence can be significant [13,15-20] and must be taken into account. The difficulty is that instrumental filter functions are hard to measure [13,16,20-24] and do not usually have a well-defined inverse. The problem of creating a control sequence that is distorted into the desired sequence is therefore ill-posed [18-20,25-27].

Here we point out that instrument filter functions do not need to be inverted or even measured precisely – we implement an extension of the GRAPE formalism that incorporates ensembles of instrument filter function cascades with user-specified parameter ranges into the optimisation loop. In this approach, only the forward action by the distortion and the Jacobian of that action are needed; both are well defined and stable. Control sequences may now be designed to be stable to multiple types of individual and sequentially applied distortions, and distributions in their parameters. We call this formalism response-aware gradient ascent pulse engineering (RAW-GRAPE) and report its implementation in versions 2.10 and later of the open-source *Spinach* library [28].

## 2. Dissipative GRAPE framework

Decoherence and return to thermal equilibrium are unavoidable; this is the principal failure modality for quantum devices. Any optimal control framework must therefore take dissipative processes into account by construction; here we use the Liouville-space (*aka* adjoint representation) version of the GRAPE framework [29,30], the unitary case is recovered by setting the relaxation superoperator to zero. In magnetic resonance notation, the general equation of motion is [31]:

$$\begin{aligned} \frac{d}{dt} \mathbf{p}(t) &= -i\mathcal{L}(t)\mathbf{p}(t), \quad \mathfrak{K}\mathbf{p} = [\mathbf{H}, \mathbf{p}] \\ \mathcal{L}(t) &= \mathfrak{K}(t) + i\mathcal{F}(t) + i\mathfrak{K}(t) + i\mathcal{R}(t) \end{aligned} \tag{1}$$

where  $\mathbf{p}$  is the density matrix,  $\mathfrak{K}(t)$  is the spin Hamiltonian commutation superoperator,  $\mathcal{F}(t)$  is the diffusion and flow generator,  $\mathfrak{K}(t)$  is the chemical kinetics superoperator, and  $\mathcal{R}(t)$  is the relaxation superoperator in which time dependence is uncommon, but may be present, for example, when the main magnet field is a function of time in low-field NMR spectroscopy and relaxometry [32].

GRAPE algorithm splits the Liouvillian  $\mathcal{L}(t)$  into the uncontrollable “drift” generator  $\mathcal{D}(t)$  and a linear combination of control generators  $\mathcal{C}_k$  whose coefficients  $c^{(k)}(t)$  the instrument can vary:

$$\mathcal{L}(t) = \mathcal{D}(t) + \sum_k c^{(k)}(t) \mathcal{C}_k \quad (2)$$

In the context of magnetic resonance spectroscopy and imaging,  $\mathcal{D}(t)$  may contain Zeeman interactions with the main magnet field, spin-spin couplings, diffusion and hydrodynamics [33], magic angle spinning [34], decoherence [35], and other processes that are beyond the possibility of agile variation. The control part may contain interactions with the fields generated by radiofrequency coil arrays, microwave resonators, and pulsed field gradient coil arrays.

Consider an experiment of duration  $T$  with the user-specified set of initial conditions  $\{\rho_0^{(m)}\}$  that must be brought into the corresponding set of desired destination states  $\{\delta^{(m)}\}$ . Depending on the size of this set, the problem may be of state-to-state type (single source and destination), subspace-to-subspace type (multiple sources-destination pairs), and gate design type (complete linearly independent set of sources-destination pairs). In all three cases, popular fidelity measures are functions of the overlap  $\Omega$  between each evolved initial condition and the corresponding target state:

$$\begin{aligned} \Omega\{\rho, \delta, \mathbf{C}\} &= \langle \delta | \overleftarrow{\exp} \left[ -i \int_0^T \mathcal{L}(t) dt \right] | \rho \rangle \\ \overleftarrow{\exp} \left( -i \int_0^t \mathcal{L}(t) dt \right) &= \lim_{\Delta t_n \rightarrow 0} \prod_n^{\leftarrow} \exp \left[ -i \mathcal{L}(t_n) \Delta t_n \right] \end{aligned} \quad (3)$$

where the arrow indicates Dyson’s time-ordered exponential [36], defined as the limit of a time-ordered product, and  $\mathbf{C}$  is the set of control sequences defined in Eq (2). GRAPE discretises this problem in time [1], the simplest case uses a set  $\{\Delta t_n\}$  of sufficiently short time intervals to approximate the drift generator and the control sequences as piecewise-constant:

$$\begin{aligned} \Omega\{\rho, \delta, \mathbf{C}\} &= \langle \delta | \mathcal{P}_N \cdots \mathcal{P}_{n+1} \mathcal{P}_n \mathcal{P}_{n-1} \cdots \mathcal{P}_1 | \rho \rangle \\ \mathcal{P}_n &= \exp \left[ -i \left( \mathcal{D}_n + \sum_k c_n^{(k)} \mathcal{C}_k \right) \Delta t_n \right] \\ c_n^{(k)}(t) &= c_n^{(k)}, \quad \mathcal{D}(t) = \mathcal{D}_n, \quad t_{n-1} \leq t < t_n \end{aligned} \quad (4)$$

What enables efficient optimisation (by gradient descent [37], conjugate gradients [38], or quasi-Newton methods [39]) is the gradient of the fidelity with respect to the control sequence. GRAPE is popular because the gradient is surprisingly cheap [2] – for each control channel  $k$  at each time step  $\Delta t_n$  only one action by the propagator derivative on a state vector is needed:

$$\frac{\partial \Omega}{\partial c_n^{(k)}} = \langle \delta | \mathcal{P}_N \cdots \mathcal{P}_{n+1} \frac{\partial \mathcal{P}_n}{\partial c_n^{(k)}} \mathcal{P}_{n-1} \cdots \mathcal{P}_1 | \rho \rangle \quad (5)$$

The equation for the propagator derivative is memorably elegant [40]:

$$\exp \left[ \begin{pmatrix} \mathbf{A} & \partial \mathbf{A} / \partial \alpha \\ \mathbf{0} & \mathbf{A} \end{pmatrix} \right] = \begin{pmatrix} e^{\mathbf{A}} & \partial e^{\mathbf{A}} / \partial \alpha \\ \mathbf{0} & e^{\mathbf{A}} \end{pmatrix} \quad (6)$$

As a result, the action by the derivative of the exponential of a matrix  $\mathbf{A}$  on a vector  $\mathbf{x}$  may be obtained simultaneously with time propagation [41] using the following block matrix relation:

$$\begin{aligned} \begin{pmatrix} [\partial e^{\mathbf{A}} / \partial \alpha] \mathbf{x} \\ e^{\mathbf{A}} \mathbf{x} \end{pmatrix} &= \begin{pmatrix} e^{\mathbf{A}} & \partial e^{\mathbf{A}} / \partial \alpha \\ \mathbf{0} & e^{\mathbf{A}} \end{pmatrix} \begin{pmatrix} \mathbf{0} \\ \mathbf{x} \end{pmatrix} = \\ &= \exp \left[ \begin{pmatrix} \mathbf{A} & \partial \mathbf{A} / \partial \alpha \\ \mathbf{0} & \mathbf{A} \end{pmatrix} \right] \begin{pmatrix} \mathbf{0} \\ \mathbf{x} \end{pmatrix} \end{aligned} \quad (7)$$

This may be efficiently computed without explicitly exponentiating the matrix [42,43]. The derivative of the evolution generator is simply a multiple of the control operator:

$$\frac{\partial}{c_n^{(k)}} \left[ -i \left( \mathfrak{D}_n + \sum_k c_n^{(k)} \mathfrak{C}_k \right) \Delta t_n \right] = -i \mathfrak{C}_k \Delta t_n \quad (8)$$

Dozens of case-specific corners may be cut at various levels of this procedure to improve the computational efficiency, sometimes by orders of magnitude [4,44-51]. At the time of writing, the most general and flexible implementation is *Spinach* [28]; the fastest no-frills implementation (single-spin Bloch equations with phase-modulated controls and without relaxation) is *SEEDLESS* [46]. A vibrant industry exists; GRAPE is a common straw to clutch at when a quantum computing architecture fails.

### 3. Distortion cascade integration into GRAPE

Consider a chain of instrumental distortions  $\rightarrow Q_1 \rightarrow Q_2 \rightarrow \dots \rightarrow Q_J \rightarrow$ , caused by every physically distinct item of hardware in the control circuit and represented here by continuous and differentiable operators  $\{Q_j\}$ . Each of them has control sequences as input and output. Our task is to account for these distortions within the GRAPE iteration loop for an ensemble of distortion parameter values; this ensemble must reflect practical variations in those parameters between instruments, samples, and measurement sessions. We assume that  $\{Q_j\}$  are easily computable and differentiable but their inverses may be ill-posed and unstable.

When distortions are present, the figure of merit and its gradient are modified by the chain rule:

$$\Omega(\mathbf{C}) \rightarrow \Omega(Q_J(\dots Q_2(Q_1(\mathbf{C})))) \quad (9)$$

$$\frac{\partial \Omega}{\partial \mathbf{C}} \rightarrow \frac{\partial \Omega}{\partial Q_J} \frac{\partial Q_J}{\partial Q_{J-1}} \dots \frac{\partial Q_2}{\partial Q_1} \frac{\partial Q_1}{\partial \mathbf{C}} \quad (10)$$

in which the chain of Jacobians is identical to the one found in backpropagation training of deep neural networks [52] – in fact, that algorithm may be re-used line for line: the forward propagation step is Eq (9), then the GRAPE gradient with respect to the output of the last distortion operation  $\partial \Omega / \partial Q_J$ , and then the chain of Jacobian multiplications in Eq (10) is the backpropagation. The difference with neural networks is that we do not optimise distortion parameters.

The user needs to supply function handles for the filter functions  $\{Q_j\}$  and their Jacobians. Alternatively (at the cost of computational efficiency), Jacobians may be obtained using automatic differentiation. Note that this approach does not require inverting any of the (in general, non-invertible) filter

functions. Thus, a complication present in some of the earlier methods dealing with instrumental distortion incorporation into GRAPE [16,18-20] is eliminated.

### 3.1 Jacobians of linear distortions

Consider first the well-researched case [16] of a distortion representable by a linear filter with a memory kernel  $h(t)$  where the input signal  $u(t)$  starts at  $t = 0$ . The output  $v(t)$  is:

$$v(t) = \int_0^t h(\tau) u(t-\tau) d\tau \quad (11)$$

When the uniform time discretisation and the piecewise-constant approximation matching Eqs (3) and (4) of the GRAPE algorithm are applied, the integral becomes (zero base indexing):

$$v_n = \sum_{m=0}^n h_m u_{n-m} \Delta t, \quad u_{k<0} = 0 \quad (12)$$

where the vector  $\mathbf{h}$  has a physical meaning of attenuation coefficients with which the system remembers its past. In terms of the input vector  $\mathbf{u}$  and the output vector  $\mathbf{v}$ , a convenient formulation of Eq (12) is  $\mathbf{v} = \mathbf{H}\mathbf{u}$  where  $\mathbf{H}$  is a Toeplitz matrix constructed from  $\mathbf{h}$ :

$$\mathbf{H} = \begin{bmatrix} h_0 & 0 & 0 & \cdots & 0 \\ h_1 & h_0 & 0 & \cdots & 0 \\ h_2 & h_1 & h_0 & \cdots & 0 \\ \vdots & \vdots & \vdots & \cdots & \vdots \end{bmatrix} \Delta t \quad (13)$$

Computing the derivatives  $\partial v_n / \partial u_k$  then demonstrates that no more work is needed: this matrix is already the Jacobian of the distortion transformation [21,22,24]. The Toeplitz form in Eq (13) is also logistically convenient because the number of non-zero elements in  $\mathbf{h}$  is usually small compared to the length of the input vector  $\mathbf{u}$ , and the matrix  $\mathbf{H}$  is therefore sparse.

### 3.2 Minimal set of linear distortions

The minimal filter set required to generate an arbitrary linear distortion by cascades and linear combinations consists of discrete single-pole (SP) and single-zero (SZ) filters with unit DC gain [53]:

$$\begin{aligned} y_n^{\text{SP}} &= (1-p)x_n + py_{n-1}^{\text{SP}} \\ y_n^{\text{SZ}} &= (x_n - zx_{n-1}) / (1-z) \end{aligned} \quad (14)$$

where  $z$  and  $p$  are dimensionless filter coefficients:

$$p = e^{-r_p \Delta t + i(\omega_p - \omega_{\text{RF}}) \Delta t}, \quad z = e^{-r_z \Delta t + i(\omega_z - \omega_{\text{RF}}) \Delta t} \quad (15)$$

that depend on the damping rates  $r_{p,z}$  and frequencies  $\omega_{p,z}$  of the pole and the zero, and on the time discretisation step  $\Delta t$ . In rotating frames (for example, with heterodyne detection at a particular frequency  $\omega_{\text{RF}}$ ),  $\omega_p$  and  $\omega_z$  are shifted by that frequency.

With cascades of these filters implemented and their Jacobians chained as shown in Eq (10), this extension of GRAPE can therefore handle an arbitrary linear distortion. We have also implemented linear combinations of cascades and their ensembles with respect to distortion parameter variations.

Figure 1 shows examples of the action by a second-order low-pass filter made by cascading two single-pole filters, a third-order high-pass filter made by cascading three single-zero filters, and an under-damped RLC circuit distortion obtained by cascading two single-pole filters.

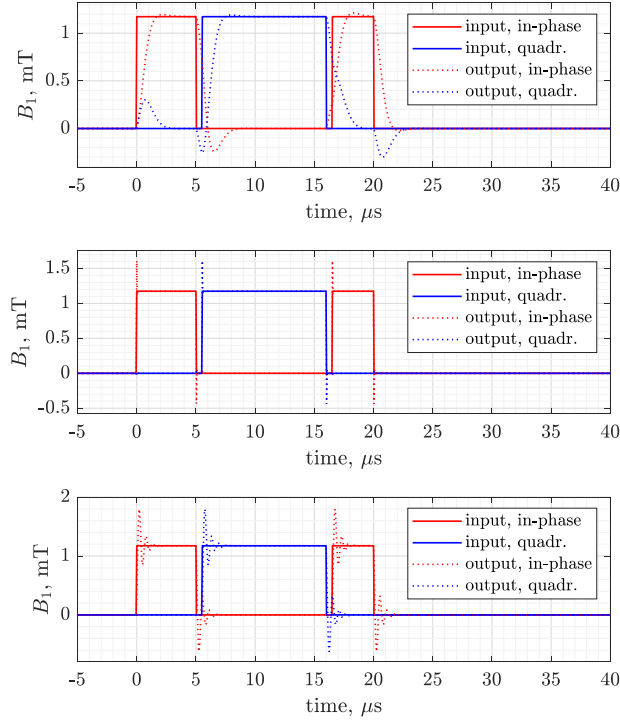


**Figure 1.** Examples of the action by cascades of single-pole and single-zero filters on the popular 90x180,90x composite inversion pulse [54], with individual pulses slightly spaced out for visual clarity and  $B_1$  field calibrated for proton Larmor frequency. **(Top Panel)** a cascade of two identical single-pole filters with the pole slightly off resonance relative to the transmitter frequency. **(Middle Panel)** a cascade of three identical single-zero filters with the zero slightly off resonance relative to the transmitter frequency. **(Bottom Panel)** an RLC circuit response filter implemented as a cascade of two single-pole filters with the opposite imaginary parts in the location of the two poles.

### 3.3 RLC circuit distortion

A practically important linear filter that deserves a special mention is the distortion introduced by an RLC circuit [20,55] with a natural frequency  $\omega$  and a quality factor  $Q$ :

$$\omega = \frac{1}{\sqrt{LC}}, \quad Q = \frac{1}{R} \sqrt{\frac{L}{C}} \quad (16)$$

This distortion (illustrated in the bottom panel of Figure 1) may be factored into a cascade of two discrete single-pole filters with the following expression for the poles [56]:

$$p_{1,2} = \exp \left( -\frac{|\omega|}{2Q} \Delta t \pm i(\omega - \omega_{\text{RF}}) \Delta t \sqrt{1 - \frac{1}{4Q^2}} \right) \quad (17)$$

where  $\Delta t$  is the time discretisation step and  $\omega_{\text{RF}}$  is the rotating frame frequency. The damping rate in this case is determined by the ratio of the natural frequency and the quality factor.

### 3.4 More complex distortions

Filter functions of control hardware may be non-linear [23,24]. Amplifiers are one example; they saturate when operating near their maximum output power. This is a common enough scourge that magnetic resonance instrument manufacturers take special measures to make their amplifiers look linear to the user and a significant body of work exists on estimating filter functions of hardware components [13,16,22]. Two simple amplitude saturation models are:

$$y = a \tanh(x/a), \quad y = x / \sqrt[s]{1 + (x/a)^s} \quad (18)$$

where  $x$  is the input amplitude,  $y$  is the output amplitude,  $a$  is the saturation level, and the sharpness of the transition from the linear to the saturating behaviour in the reciprocal root model is regulated by the parameter  $s > 1$ . Figure 2 shows the effect of amplifier saturation described by Eq (18) on a popular Veshtort-Griffin E1000B radiofrequency pulse [57] that performs band-selective excitation in magnetic resonance spectroscopy.

In general, non-linear distortions are hardware- and system-specific; a software implementation cannot anticipate any properties other than the model being differentiable. At the software level we have therefore opted for automatic differentiation: users need only to supply the function itself; the Jacobian is generated using the `dljacobian.m` function of *Matlab's* Deep Learning Toolbox [58].

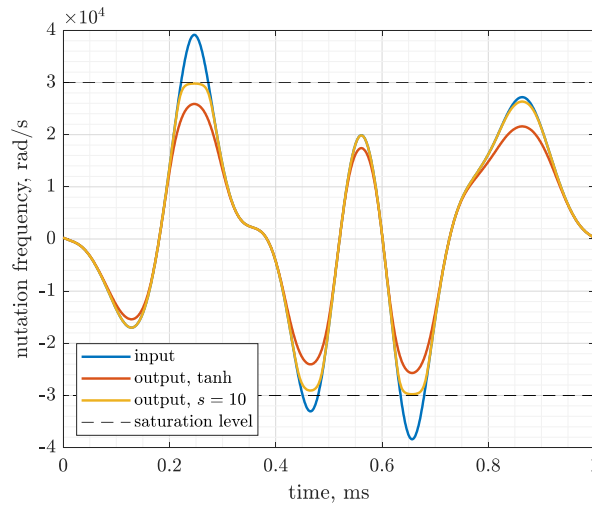


**Figure 2.** An example of the amplifier compression effect, computed using Eq (18), on a Veshtort-Griffin E1000B radiofrequency pulse used in NMR spectroscopy to achieve band-selective magnetisation excitation [57].

Common hardware non-linearities provided as templates with *Spinach* package [28] are:

**Phase distortions.** These originate from dispersive effects of filters, cables, and connectors, and from other hardware that introduces frequency-dependent phase shifts [59].

**Frequency-dependent attenuation.** Hardware components can attenuate specific frequencies; high frequencies are particularly vulnerable due to skin effects and dielectric losses [60].

**Nonlinear crosstalk.** This occurs when signals in spatially adjacent components interfere nonlinearly, producing intermodulation products; cross-talk is particularly problematic in compact systems and integrated circuits, where channels are hard to isolate [61].

**Signal timing errors.** Sample timing errors in digital signals can effectively shift frequencies and introduce irreproducible additional modulations [62].

**Digital quantisation:** Analogue-to-digital and digital-to-analogue converters approximate continuous signals using discrete levels; this quantisation can manifest as a noise source [56].

To generalise the procedures and functions above to arbitrary differentiable distortions, we use a well-known result from machine learning: the universal approximator theorem, which states that a sufficiently long superposition of linear transformations with element-wise non-linearities can approximate any Borel measurable map between vector spaces to any accuracy [63]. We therefore conclude that, at least in principle, any instrumental distortion can be accommodated within GRAPE using cascades, linear combinations, and ensembles of the basic components described above.

#### 4. Performance illustrations

To illustrate the performance of the RAW-GRAPE approach, we consider universal rotation pulse design – a common problem in magnetic resonance [64] and atom interferometry [11]. We model typical hardware distortions seen in those spectroscopies: probe circuit ringing and amplifier saturation. As magnetic resonance fields get higher (at the time of writing, cutting-edge NMR instruments run at 28.18 Tesla), optimal control methods become unavoidable [14,44,64] because hard inversion pulses are not instrumentally possible: commonly available RF nutation frequencies in latest cryoprobes at 28.18 Tesla are 20 kHz on  $^1\text{H}$ , 15 kHz on  $^{13}\text{C}$ , and 5 kHz on  $^{15}\text{N}$ . Throughout this section we use simulated performance profiles interchangeably with experimental data; this is warranted in magnetic resonance because simulation methods are exceptionally well developed and provide a close match.

Our universal rotation pulse must accomplish the following transformation of single-spin density matrices (for spin 1/2, these are Pauli matrices scaled to have  $[\mathbf{S}_x, \mathbf{S}_y] = i\mathbf{S}_z$ ):

$$\mathbf{S}_z \rightarrow \mathbf{S}_x, \quad \mathbf{S}_y \rightarrow \mathbf{S}_y, \quad \mathbf{S}_x \rightarrow -\mathbf{S}_z \quad (19)$$

within a given chemical shift range (we chose 200 ppm for  $^{13}\text{C}$  in a 28.18 Tesla magnet). The pulse must be short enough for the worst-case  $^{13}\text{C}$ - $^1\text{H}$   $J$ -coupling (around 200 Hz) to have a negligible effect; this caps the duration at about  $1/100J = 50 \mu\text{s}$ . Maximum instrumentally achievable  $^{13}\text{C}$  nutation frequency in a room temperature NMR probe varies from 50 to 70 kHz across the radiofrequency coil of the NMR probe, and therefore a hard  $^{13}\text{C}$  pulse (*i.e.* the shortest pulse at the maximum available RF power, here about 4  $\mu\text{s}$ ) yields significant phase errors across the spectral window (Figure 3, top left).

For room temperature NMR probes (Q-factors between 50 and 200), this can be overcome using optimal control (Figure 3, bottom left) with the additional advantage of lower pulse power [14,44,64]. However, stronger RLC circuit distortions render such pulses ineffectual: when the circuit quality factor is increased into thousands (corresponding to a narrowly optimised cryoprobe [55]), the fidelity of the pulse degrades (Figure 3, top right). At that point, introducing RLC distortion modelling into the GRAPE



loop as described above eliminates the problem: when RAW-GRAPE is used, the performance of the RLC distorted pulse returns to the high fidelity (Figure 3, bottom right).

At the software implementation level, we have condensed the procedures described above into just one additional user input line in the optimal control module of the *Spinach* package [51]:

```
% Add RLC distortion to the GRAPE workflow
control.distortion = { @(w)spf(w,p1), @(w)spf(w,p2) };
```

Here, the distortion cascade is specified as a cell array of *Matlab* function handles. The functions are both SPF (single pole filter, supplied with *Spinach*) and their parameters  $p_1$  and  $p_2$  are the two filter coefficients from Eq (17), where  $\omega$  is the Larmor frequency of  $^{13}\text{C}$  and the quality factor  $Q$  is set by the user. A number of other distortion functions are provided with *Spinach* kernel, and more can be added by the user in a matter of minutes because *Matlab* takes care of the Jacobian calculation.

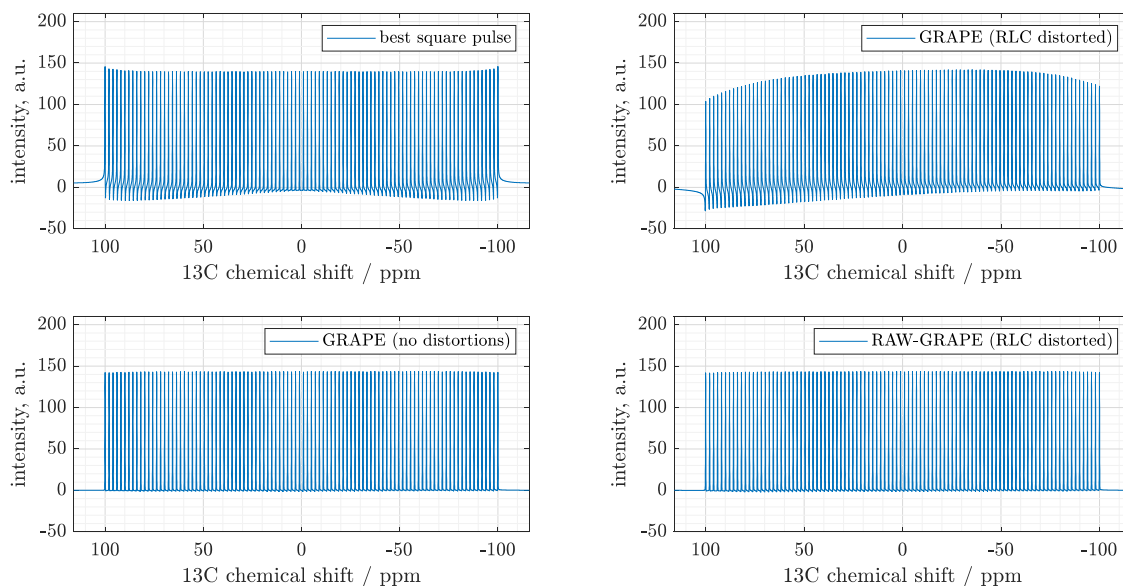


**Figure 3.** Performance comparison for the universal rotation pulses intended to accomplish the state space transformation in Eq (19) for an ensemble of 100  $^{13}\text{C}$  nuclei spread uniformly over a  $\pm 100$  ppm interval in a 28.18 Tesla (1.2 GHz proton frequency) NMR magnet. The shortest instrumentally available square pulse (**Top Left**) yields unavoidable phase distortions caused by the sinc bands of the pulse. An optimal control pulse designed using GRAPE is able to eliminate those distortions (**Bottom Left**), but the optimal pulse remains vulnerable to the effect of the RLC filter function of the probe circuit ( $Q=1000$ , **Top Right**). Using the RAW-GRAPE optimal control algorithm, where hardware distortion modelling is a part of the optimisation loop, eliminates the problem (**Bottom Right**). The script generating this figure is available in the example set supplied with versions 2.10 and later of *Spinach*.

An important aspect of quantum control is that different instruments and samples may have different distortion parameters. In bad cases, those parameters may not be the same from one experiment to the next, and may even vary across the sample – a famous case is radiofrequency field inhomogeneity within magnetic resonance coils and resonators [65]. It is therefore important to generate pulses that are resilient to ranges of instrumental distortion parameters. We have implemented this as an instance of ensemble control because ensemble handling is already available within *Spinach* library [51].

At the input syntax level, an ensemble of distortion cascades is supplied as multiple rows of the distortion function handle array, for example:

```
% Add ensemble of RLC distortions to the GRAPE workflow
control.distortion = { @(w)spf(w,p1(1)), @(w)spf(w,p2(1))
                      @(w)spf(w,p1(2)), @(w)spf(w,p2(2))
                      ...
                      @(w)spf(w,p1(n)), @(w)spf(w,p2(n)) };
```

where p1 and p2 are now arrays. This tells *Spinach* to create an ensemble of systems (parallelisation over ensembles is automatic) and to maximise the average fidelity across the ensemble.

Optimal control pulses generated using this procedure are resilient to ranges of distortion parameter values; this is illustrated in Figure 4 for two bi-parametric ensembles: power and RLC quality factor in the top panel, power and saturation level in the bottom panel.

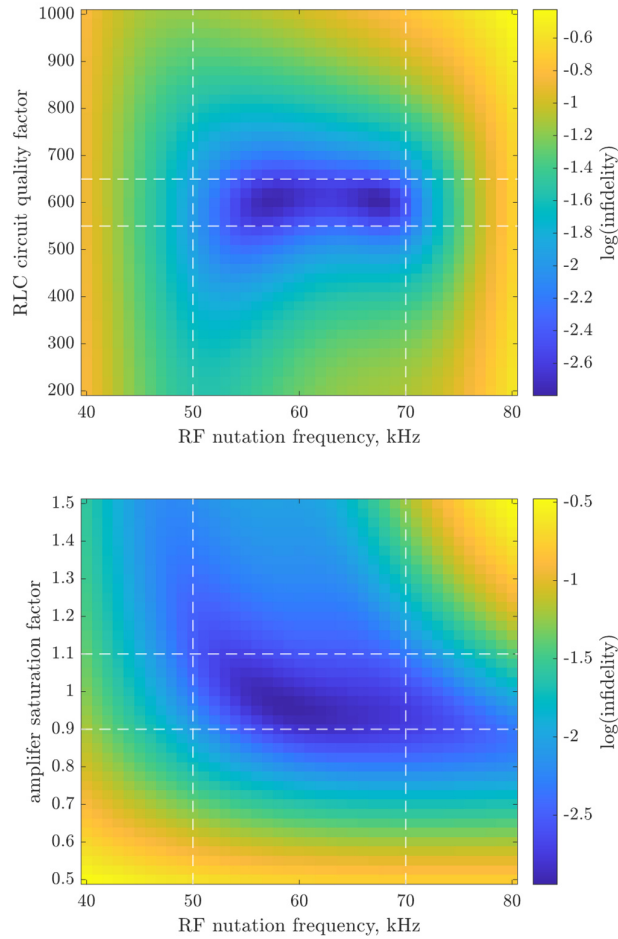


**Figure 4.** Infidelity of the optimised universal rotation pulse (see Section 4 and Figure 3 caption for the parameters) in the presence of biparametric distortion ensembles. The pulse was optimised, using RAW-GRAPE, to be resilient to RF nutation frequency variations between 50 and 70 kHz, RLC quality factors variations between 560 and 640, and amplifier saturation levels between 50% to 150% of the maximum pulse power. Dashed lines in all panels indicate the distortion parameter ranges. **(Top Panel)** Biparametric ensemble of distortions (quality factor, nutation frequency) and the performance of the resulting pulse. **(Bottom Panel)** Biparametric ensemble of distortions (amplifier saturation level, nutation frequency) and the performance of the resulting pulse.

Another important aspect of ensemble control is the trade-off between the fidelity that could have been achieved with fixed distortion parameters (sacrificed) and worst-case fidelity across the distortion parameter ensemble (improved). This is important for designing optimal control pulses that are transferable between instruments, samples, and measurement session. Figure 5 illustrates this principle in the same magnetic resonance settings: although RAW-GRAPE fidelity drops in the cases when distortions are benign, it does not then drop quite as much when distortions become significant.

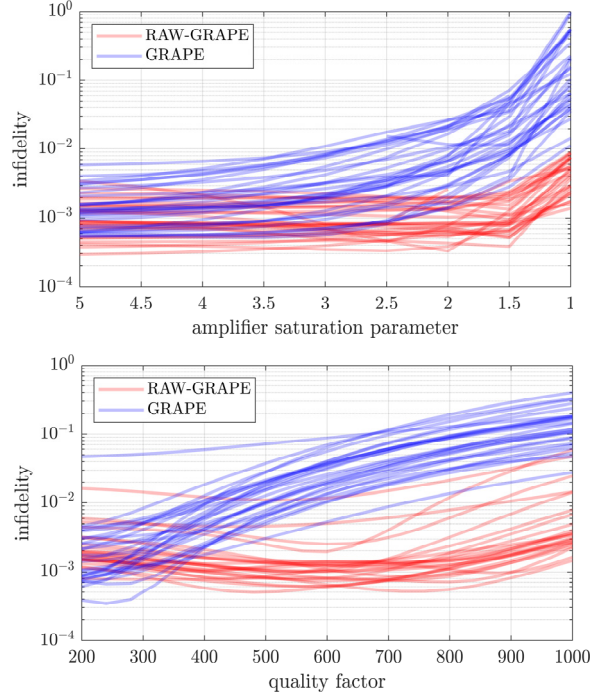


**Figure 5.** Performance illustrations (using "spaghetti plots" of multiple optimisation runs from different random initial guess pulses) for RAW-GRAPE (red lines) and original GRAPE (blue lines) in optimising a universal rotation pulse described in Section 4. (**Top Panel**) Ensemble of amplifier saturation levels, from negligible distortion when the ceiling is at 5 times the pulse power to strong distortion when the pulse is touching the ceiling. (**Bottom Panel**) Ensemble of NMR probe circuit quality factors, from negligible distortions at  $Q=200$  (e.g. highly tuned room temperature probe) to strong distortion at  $Q=1000$  (e.g. highly tuned specialised cryoprobe).

## 5. Conclusions and outlook

In the context of quantum optimal control, a significant problem is control sequence distortion by instrument electronics and optics [5,13,16,20,24,26,27]. Inverse transformations of those distortions may be ill-defined and unstable. However, inverting distortion functions is not actually necessary within the gradient ascent pulse engineering (GRAPE) framework for quantum optimal control – the only requirement is that a continuous Jacobian should exist; the rest of the mathematics is then reminiscent of the backpropagation algorithm used in artificial intelligence.

Using the algorithms described above, we have implemented arbitrary cascades of arbitrary differentiable distortions, and the corresponding ensemble control extensions, into version 2.10 of the open-source *Spinach* library, where the algorithm is called Response-AWare GRAPE (RAW-GRAPE for short). The user needs to supply function handles for the distortions; Jacobians are obtained internally using

automatic differentiation. A set of common distortions (single-pole filter, single-zero filter, amplifier compression) is provided, those functions also serve as templates for customisation.

RAW-GRAPE improves robustness of optimal control sequences in situations where cascades and ensembles of instrumental distortions exist that are non-negligible and variable between instruments, samples, and measurement sessions.

## Acknowledgements

This work was supported by a research grant from the Centre for New Scientists at the Weizmann Institute of Science, by EPSRC (EP/Y035267/1) and MathWorks (who sponsored UR's PhD studentship), and used NVIDIA Tesla A100 GPUs through NVIDIA Academic Grants Programme. IK is indebted to the Weizmann Institute of Science for rescuing him from the crushing undergraduate teaching and administration workload at Southampton that would otherwise have made this work impossible.

## References

1. Khaneja, N., T. Reiss, C. Kehlet, T. Schulte-Herbrüggen, and S.J. Glaser, *Optimal control of coupled spin dynamics: design of NMR pulse sequences by gradient ascent algorithms*. Journal of Magnetic Resonance, 2005. **172**(2): p. 296-305.
2. de Fouquieres, P., S.G. Schirmer, S.J. Glaser, and I. Kuprov, *Second order gradient ascent pulse engineering*. Journal of Magnetic Resonance, 2011. **212**(2): p. 412-417.
3. Goodwin, D.L. and I. Kuprov, *Modified Newton-Raphson GRAPE methods for optimal control of spin systems*. Journal of Chemical Physics, 2016. **144**(20): p. 204107.
4. Vinding, M.S., D.L. Goodwin, I. Kuprov, and T.E. Lund, *Optimal control gradient precision trade-offs: Application to fast generation of DeepControl libraries for MRI*. Journal of Magnetic Resonance, 2021. **333**: p. 107094.
5. Rasulov, U., A. Acharya, M. Carravetta, G. Mathies, and I. Kuprov, *Simulation and design of shaped pulses beyond the piecewise-constant approximation*. Journal of Magnetic Resonance, 2023. **353**.
6. Coote, P., W. Bermel, and H. Arthanari, *Optimization of phase dispersion enables broadband excitation without homonuclear coupling artifacts*. Journal of Magnetic Resonance, 2021. **325**: p. 106928.
7. Joseph, D. and C. Griesinger, *Optimal control pulses for the 1.2-GHz (28.2-T) NMR spectrometers*. Science Advances, 2023. **9**.
8. Massire, A., M. Cloos, A. Vignaud, D. Bihan, A. Amadon, and N. Boulant, *Design of non-selective refocusing pulses with phase-free rotation axis by gradient ascent pulse engineering algorithm in parallel transmission at 7 T*. Journal of Magnetic Resonance, 2013. **230**.
9. Egger, D.J. and F.K. Willhelm, *Optimized controlled-Z gates for two superconducting qubits coupled through a resonator*. Superconductor Science and Technology, 2013. **27**.
10. Saywell, J., M. Carey, M. Belal, I. Kuprov, and T. Freegarde, *Optimal control of Raman pulse sequences for atom interferometry*. Journal of Physics B, 2020. **53**(8): p. 085006.
11. Saywell, J., M. Carey, I. Kuprov, and T. Freegarde, *Biselective pulses for large-area atom interferometry*. Physical Review A, 2020. **101**(6): p. 063625.

12. Skinner, T.E., M. Braun, K. Woelk, N.I. Gershenzon, and S. Glaser, *Design and application of robust rf pulses for toroid cavity NMR spectroscopy*. Journal of Magnetic Resonance, 2011. **209**(2).
13. Goodwin, D.L., W.K. Myers, C.R. Timmel, and I. Kuprov, *Feedback control optimisation of ESR experiments*. Journal of Magnetic Resonance, 2018. **297**: p. 9-16.
14. Skinner, T.E., T.O. Reiss, B. Luy, N. Khaneja, and S.J. Glaser, *Application of optimal control theory to the design of broadband excitation pulses for high-resolution NMR*. Journal of Magnetic Resonance, 2003. **163**(1): p. 8-15.
15. Tošner, Z., R. Sarkar, J. Becker-Baldus, C. Glaubitz, S. Wegner, F. Engelke, S.J. Glaser, and B. Reif, *Overcoming Volume Selectivity of Dipolar Recoupling in Biological Solid-State NMR Spectroscopy*. Angewandte Chemie International Edition, 2018. **57**(44): p. 14514-14518.
16. Spindler, P.E., Y. Zhang, B. Endeward, N. Gershenzon, T.E. Skinner, S.J. Glaser, and T.F. Prisner, *Shaped optimal control pulses for increased excitation bandwidth in EPR*. Journal of Magnetic Resonance, 2012. **218**: p. 49-58.
17. Spindler, P.E., P. Schöps, W. Kallies, S.J. Glaser, and T.F. Prisner, *Perspectives of shaped pulses for EPR spectroscopy*. Journal of Magnetic Resonance, 2017. **280**: p. 30-45.
18. Probst, S., V. Ranjan, Q. Ansel, R. Heeres, B. Albanese, E. Albertinale, D. Vion, D. Esteve, S.J. Glaser, D. Sugny, and P. Bertet, *Shaped pulses for transient compensation in quantum-limited electron spin resonance spectroscopy*. Journal of Magnetic Resonance, 2019. **303**: p. 42-47.
19. Wittmann, J.J., K. Takeda, B.H. Meier, and M. Ernst, *Compensating Pulse Imperfections in Solid-State NMR Spectroscopy: A Key to Better Reproducibility and Performance*. Angewandte Chemie International Edition, 2015. **54**(43): p. 12592-12596.
20. Borneman, T.W. and D.G. Cory, *Bandwidth-limited control and ringdown suppression in high-Q resonators*. Journal of Magnetic Resonance, 2012. **225**: p. 120-129.
21. Motzoi, F., J.M. Gambetta, S.T. Merkel, and F.K. Wilhelm, *Optimal control methods for rapidly time-varying Hamiltonians*. Physical Review A, 2011. **84**(2): p. 022307.
22. Sørensen, J.J., J.S. Nyemann, F. Motzoi, J. Sherson, and T. Vosegaard, *Optimization of pulses with low bandwidth for improved excitation of multiple-quantum coherences in NMR of quadrupolar nuclei*. Journal of Chemical Physics, 2020. **152**(5).
23. Singh, J., R. Zeier, T. Calarco, and F. Motzoi, *Compensating for Nonlinear Distortions in Controlled Quantum Systems*. Physical Review Applied, 2023. **19**(6): p. 064067.
24. Hincks, I., C. Granade, T.W. Borneman, and D.G. Cory, *Controlling quantum devices with nonlinear hardware*. Physical Review Applied, 2015. **4**(2): p. 024012.
25. Tikhonov, A.N. and V.Y. Arsenin, *Solutions of Ill-Posed Problems*, ed. W.a. Sons. 1977.
26. Cao, X., B. Chu, Y.-X. Liu, Z. Peng, and R.-B. Wu, *Learning to calibrate quantum control pulses by iterative deconvolution*. IEEE Transactions on Control Systems Technology, 2021. **30**(1): p. 193-201.
27. Åkesson, A.T. and M. Kjærgaard, *MSc Thesis: Correcting Control Pulse Distortions in Superconducting Qubits*. University of Copenhagen, 2022.
28. Hogben, H.J., M. Krzystyniak, G.T. Charnock, P.J. Hore, and I. Kuprov, *Spinach – a software library for simulation of spin dynamics in large spin systems*. Journal of Magnetic Resonance, 2011. **208**(2): p. 179-194.
29. Bain, A.D. and J.S. Martin, *FT NMR of nonequilibrium states of complex spin systems, Part I: a Liouville space description*. Journal of Magnetic Resonance, 1978. **29**(1): p. 125-135.

30. Banwell, C. and P. H., *On the analysis of high-resolution nuclear magnetic resonance spectra, Part I: methods of calculating NMR spectra*. Molecular Physics, 1963. **6**.
31. von Neumann, J., *Wahrscheinlichkeitstheoretischer aufbau der quantenmechanik*, Nachrichten von der Gesellschaft der Wissenschaften zu Göttingen. Math.-Phys., 1927. **Klasse 245–272**.
32. Kowalewski, J. and L. Maler, *Nuclear Spin Relaxation in Liquids: Theory, Experiments, and Applications*, ed. T. Francis. 2006, London.
33. Torrey, H.C., *Bloch equations with diffusion terms*. Physical Review, 1956. **104**.
34. Andrew, E.R., A. Bradbury, and R.G. Eades, *Removal of Dipolar Broadening of Nuclear Magnetic Resonance Spectra of Solids by Specimen Rotation*. Nature, 1959. **183**.
35. Abragam, A., *The principles of nuclear magnetism* ed. O.S. Publications. 1961.
36. Dyson, F.J., *The radiation theories of Tomonaga, Schwinger, and Feynman*. Physical Review, 1949. **75**(3): p. 486-502.
37. Cauchy, A., *Méthode générale pour la résolution des systemes d'équations simultanées*. Comp. Rend. Sci. Paris, 1847. **25**(1847): p. 536-538.
38. Hestenes, M. and S. E., *Methods of Conjugate Gradients for Solving Linear Systems*. Journal of Research of the National Bureau of Standards, 1952. **49**.
39. Broyden, C.G., *Quasi-Newton methods and their application to function minimisation*. Mathematics of Computation, 1967. **21**.
40. Goodwin, D.L. and I. Kuprov, *Auxiliary matrix formalism for interaction representation transformations, optimal control, and spin relaxation theories*. Journal of Chemical Physics, 2015. **143**(8): p. 084113.
41. Kuprov, I. and C.T. Rodgers, *Derivatives of spin dynamics simulations*. Journal of Chemical physics, 2009. **131**(23).
42. Sidje, R.B., *Expokit: a software package for computing matrix exponentials*. ACM Transactions on Mathematical Software, 1998. **24**(1): p. 130-156.
43. Kuprov, I., *Coherent Spin Dynamics*, in *Spin: From Basic Symmetries to Quantum Optimal Control*. 2023, Springer. p. 107-179.
44. Gershenson, N.I., K. Kobzar, B. Luy, S.J. Glaser, and T.E. Skinner, *Optimal control design of excitation pulses that accommodate relaxation*. Journal of Magnetic Resonance, 2007. **188**(2): p. 330-336.
45. Vinding, M.S., I.I. Maximov, Z. Tošner, and N.C. Nielsen, *Fast numerical design of spatial-selective rf pulses in MRI using Krotov and quasi-Newton based optimal control methods*. Journal of Chemical Physics, 2012. **137**(5).
46. Buchanan, C., G. Bhole, G. Karunanithy, V. Casablanco-Antràs, A. Poh, B. Davis, J. Jones, and A. Baldwin, *Seedless: On-the-fly pulse calculation for NMR experiments*. <https://www.biorxiv.org/content/10.1101/2024.01.31.578133v1>, 2024.
47. Tošner, Z., T. Vosegaard, C. Kehlet, N. Khaneja, S.J. Glaser, and N.C. Nielsen, *Optimal control in NMR spectroscopy: numerical implementation in SIMPSON*. Journal of Magnetic Resonance, 2009. **197**(2): p. 120-134.
48. Baldwin, A.J. and J.A. Jones, *Efficiently computing the Uhlmann fidelity for density matrices*. Physical Review A, 2023. **107**(1): p. 012427.
49. Bhole, G., T. Tsunoda, P.J. Leek, and J.A. Jones, *Rescaling Interactions for Quantum Control*. Physical Review Applied, 2020. **13**(3): p. 034002.

50. Goodwin, D.L. and M.S. Vinding, *Accelerated Newton-Raphson GRAPE methods for optimal control*. Physical Review Research, 2023. **5**(1): p. L012042.
51. Kuprov, I., *Optimal control of spin systems*, in *Spin: From Basic Symmetries to Quantum Optimal Control*. 2023, Springer. p. 313-349.
52. Rumelhart, D., G. Hinton, and R. Williams, *Learning representations by back-propagating errors*. Nature, 1986. **323**.
53. Oppenheim, A.V., A. Willsky, and H. Nawab, *Signals and Systems*. 1996: Prentice-Hall.
54. Levitt, M.H., *Composite pulses*. Progress in Nuclear Magnetic Resonance Spectroscopy, 1986. **18**(2): p. 61-122.
55. Thomas, J., T. Johnston, I. Litvak, V. Ramaswamy, M. Merritt, J. Rocca, A. Edison, and W. Brey. *Implementing high Q-factor HTS resonators to enhance probe sensitivity in  $^{13}\text{C}$  NMR spectroscopy*. in *Journal of Physics: Conference Series*. 2022. IOP Publishing.
56. Proakis, G. and D.G. Manolakis, *Digital Signal Processing: Principles, Algorithms, and Applications*. 2007: Pearson/Prentice Hall.
57. Veshtort, M. and R.G. Griffin, *High-performance selective excitation pulses for solid- and liquid-state NMR spectroscopy*. ChemPhysChem, 2004. **5**(6): p. 834-850.
58. The MathWorks Inc., *Deep Learning Toolbox (Matlab R2024b)*. 2024: Natick, Massachusetts, United States.
59. Pozar, D.M., *Microwave Engineering, 4th Edition*. 2012: Wiley.
60. Webb, A., *Magnetic Resonance Technology: Hardware and System Component Design*. Royal Society of Chemistry. 2016.
61. Roemer, P.B., W.A. Edelstein, C.E. Hayes, S.P. Souza, and O.M. Mueller, *The NMR phased array*. Magn Reson Med, 1990. **16**.
62. Hall, S., G. Hall, and A. McCall, *High-Speed Digital System Design: A Handbook of Interconnect Theory and Design Practices*. 2000: John Wiley & Sons, Inc.
63. Hornik, K., M. Stinchcombe, and H. White, *Multilayer feedforward networks are universal approximators*. Neural Networks, 1989. **2**(5): p. 359-366.
64. Kyril Kobzar, Sebastian Ehni, Thomas E. Skinner, Steffen J. Glaser, and Burkhard Luy, *Exploring the limits of broadband  $90^\circ$  and  $180^\circ$  universal rotation pulses*. Journal of Magnetic Resonance, 2012. **225**.
65. Tošner, Z., M.J. Brandl, J. Blahut, S.J. Glaser, and B. Reif, *Maximizing efficiency of dipolar recoupling in solid-state NMR using optimal control sequences*. Science advances, 2021. **7**(42): p. eabj5913.